



The Greenland Firn Compaction Verification and Reconnaissance (FirnCover) Dataset, 2013-2019

5 Michael J. MacFerrin¹, C. Max Stevens^{2,3,4}, Baptiste Vandecrux⁵, Edwin D. Waddington², Waleed Abdalati¹

¹Cooperative Institute for Research in Environmental Sciences (CIRES), University of Colorado, Boulder, CO, USA

²Department of Earth and Space Sciences, University of Washington, Seattle, WA, USA

³NASA Goddard Space Flight Center, Greenbelt, MD, USA

⁴Earth System Science Interdisciplinary Center, University of Maryland, College Park, MD, USA

10 ⁵Geological Survey of Denmark and Greenland, Copenhagen, Denmark

Correspondence to Michael J. MacFerrin (michael.macferrin@colorado.edu)

Abstract. Assessing changes in the density of snow and firn is vital to convert volume changes into mass changes on glaciers and ice sheets. Firn models simulate this process but typically rely upon steady-state assumptions and geographically and temporally limited sets of field measurements for validation. Given rapid changes recently observed in Greenland's surface mass balance, a contemporary dataset measuring firn compaction in a range of climate zones across the Greenland ice sheet's accumulation zone is needed. To fill this need, the Firn Compaction Verification and Reconnaissance (FirnCover) dataset comprises daily measurements from 50 strainmeters installed in boreholes at eight sites on the Greenland ice sheet between 15 2013 and 2019. The dataset also includes daily records of two-meter air temperature, snow height, and snow temperature from each station. The majority of the FirnCover stations were installed in close proximity to automated weather stations that measure a wider suite of meteorological measurements, allowing the user access to auxiliary datasets for model validation 20 studies using FirnCover data. The dataset can be found here: <https://www.doi.org/10.18739/A25X25D7M> (MacFerrin et al., 2021).

25 1. Introduction

Mass loss from the Greenland ice sheet (GrIS) is currently one of the largest direct contributors to sea-level rise (IPCC, 2013), and the majority of that loss since the early 2000s has been due to significant increases in surface melt and runoff (Velicogna et al., 2014, van den Broeke et al., 2016; Mottram et al., 2019). In Greenland's accumulation zone, which covers approximately 80% of the ice sheet (Box et al., 2006), annual snow accumulation is buried and densifies until it becomes glacial ice (Bader, 1954; Benson, 1962; Herron and Langway, 1980). Greenland's firn layer can be up to ~70 m thick (Schwander et al., 1997). 30



The GrIS's firn layer has been the subject of recent research for multiple reasons. First, assessments of Greenland's total mass balance using altimetry products use satellite-derived measurements of surface height to assess ice sheet volume, but need to resolve the evolution of the firn's porosity before converting volume change into mass change (i.e. Zwally et al., 2011; Shepherd et al., 2012; Csatho et al., 2014; McMillan et al., 2016, Smith et al., 2020). Second, the firn is able to retain part of the meltwater generated at the surface and buffer sea level rise (Pfeffer et al., 1991). The firn's retention capacity depends on both the pore volume available for meltwater storage (Harper et al., 2012), which is decreasing (Vandecrux et al, 2019), and the firn's cold content, which is the energy required to bring the firn to the melting temperature (Vandecrux et al., 2020). Third, near-surface ice slabs have formed in western Greenland's firn. These slabs block percolation and reduce the buffering capacity, and thus promote lateral runoff (Machguth et al., 2016, MacFerrin et al. 2019). The development of these features is the result of increased melt volume (MacFerrin et al. 2019), increased near-surface firn densities, and sufficient cold content to sustain meltwater refreezing (Vandecrux et al., 2020). Finally, knowing the depth and age of the firn-ice transition is important for the interpretation of climate records from ice cores (Schwander and Stauffer, 1984; Adolf and Albert., 2014). In all these cases, knowledge of the firn's compaction rate is crucial, yet to date there are relatively few in situ measurements of firn compaction, and there is no single, widely accepted model to simulate it. In this paper, we present the Firn Compaction Verification and Reconnaissance (FirnCover) dataset, which comprises measurements of firn compaction, depth-density profiles, and temperatures from eight sites on the GrIS.

2. Background

Firn densification characterizes a general increase of the firn's bulk density and encompasses multiple processes. *Firn compaction* refers specifically to the compression of the firn due to overburden stress. Firn compaction occurs due to processes operating at the grain scale such as grain boundary sliding, sintering mechanisms including dislocation creep and lattice diffusion, and plastic deformation (Herron and Langway, 1980; Morris and Wingham, 2014). *Meltwater refreezing* increases the firn density when surface meltwater or rain refreezes in the firn's pore space. This occurs primarily in the warmest regions of the ice sheet's accumulation area. The two above-mentioned phenomena are interconnected because meltwater refreezing releases latent heat and increases the firn temperature, which accelerates compaction of surrounding firn. In the highest-elevation zones of the ice sheet, where firn densification mainly occurs through compaction, the compaction rate in the near-surface firn varies seasonally due to the fluctuating temperature; the deeper firn does not experience this seasonal variation in compaction rate. Long-term changes in climate (temperature and accumulation rate) may take many decades before they affect compaction rates over the full depth of the firn column (Li and Zwally, 2015). In the percolation zone, the seasonal cycle in near-surface firn compaction rate is also present. However, the infusion of meltwater can change the compaction rate on much shorter timescales (days to weeks) as latent heat rapidly warms the firn, and rapid densification can occur when the refrozen meltwater fills the pore space. This firn may then compact more slowly in the future because of its higher density. In this realm, a single anomalous melt season can significantly affect the depth-density profile (Brown et al., 2012).



65 Numerous models have been developed to simulate firn compaction and densification on various time scales (e.g. Herron and
Langway, 1980; Arnaud et al., 2000; Zwally et al., 2011, Arthern et al., 2010; Ligtenberg et al., 2011; Morris et al., 2014). On
yearly and longer time scales, firn depth-density profiles and compaction rates can be estimated reasonably well using the
mean annual air temperatures and accumulation rates (Herron and Langway, 1980). These firn-model results can be used e.g.
to simulate the long-term evolution of the firn-ice transition depth for ice-core studies (Goujon et al., 2003; Rasmussen et al.,
70 2013). On shorter (monthly, daily, or sub-daily) time scales, firn models can be forced with weather data and/or outputs from
regional climate models (RCMs) to simulate the firn temperature, density, and thickness change (Vandecrux, et al., 2020).
Results from these model runs can be used to correct repeat surface-elevation measurements from altimetry for firn changes
(e.g. Smith et al., 2020). Numerous recent studies have coupled meltwater-percolation schemes to firn-compaction models
(e.g. Reeh, 2008; Kuipers-Munneke et al., 2015; Vionnet et al., 2012; van Pelt et al., 2016; Verjans et al., 2019; Vandecrux et
75 al., 2020) to simulate liquid water content, refreezing, and runoff in the firn.

Most firn-densification schemes have generally been developed using density profiles observed in firn cores (Herron and
Langway, 1980; Sørensen et al., 2011; Kuipers-Munneke et al., 2015). By assuming that the firn is in steady state, a dated
depth-density profile can be converted to a densification rate. There are several potential issues with this method. First, it is
80 not necessarily safe to assume that the firn at a given site is in steady state. Even if the firn is in steady state, a compaction rate
derived from the depth-density profile does not provide information about the firn's response to a transient climate or how its
compaction rate varies on sub-annual timescales. Additionally, density profiles from the percolation zone cannot disentangle
contributions of firn compaction and meltwater refreezing, which makes it difficult to assess these two processes in firn models.
Finally, a densification model that is tuned to match firn-density observations may be biased if there are errors or biases in the
85 climate forcing that is used to tune the model.

Among the numerous firn models, none is broadly accepted as a definitive model. Lundin et al. (2017) showed that these
models agree neither in steady-state nor in transient modes. Further, certain firn models are tuned specifically for Greenland
or Antarctica, despite the fact that the physical processes driving densification should not vary solely due to geographic
90 location. Vandecrux et al. (2020) compared numerous firn-meltwater models to observations and found that while different
models accurately simulated physical characteristics of different firn zones in Greenland, no single model accurately
represented firn density, temperature and water content at all sites.

The uncertainties associated with firn-model development and the disagreement among the existing models underscore the
95 need for direct measurements of firn compaction. Such measurements are currently rare and from only isolated regions of an
ice sheet (Hamilton et al., 1998; Arthern et al., 2010; Morris and Wingham 2014; Hubbard et al. 2020).



To fill this knowledge gap and increase our understanding of firn densification, we present data from the Firn Compaction Verification and Reconnaissance (FirnCover) project, which monitored firn compaction between 2013 and 2019 at eight stations on the GrIS. Each station monitors firn compaction with strainmeters installed over boreholes at various depth ranges, as well as firn temperature, air temperature and surface height. Additionally, we measured depth-density and stratigraphy profiles of recovered cores and in snow pits during each field visit. In this paper, we describe the FirnCover stations (Section 3) and the dataset organization (Section 4), and then we present a preliminary analysis of the dataset (Section 5).

3. The FirnCover stations and dataset

The eight FirnCover stations are located in various climate zones of the ice sheet accumulation area (Figure 1, Table 1). Two stations, Summit and EastGrip, are located in the high-elevation, dry-snow zone of the ice sheet, where melt rarely occurs and where firn compaction is the dominant densification process. Six stations are located in the percolation zone of the ice sheet, where changes in surface meltwater and refreezing are changing the structure and density profiles of firn (MacFerrin et al., 2019; Machguth et al., 2016; Vandecrux et al., 2018). The KAN_U, Dye-2, and EKT stations were installed in Spring 2013 and the remainder of the stations in Spring 2015. At every station, additional instruments were installed in new boreholes upon subsequent visits.

Each station included a suite of instruments, which we detail below, and was equipped with a tower to hold instrumentation, a data logger (Campbell CR800), a solar panel, and a battery. Borehole strain rates were recorded daily, while air temperature, surface height, and firn temperature measurements were recorded hourly. During most years, summary data from the instruments was transmitted from each station once per day using an Iridium short-burst data modem. Full data tables were saved on the data logger and were read from each station upon visits in the field, which usually occurred in late April or early May.

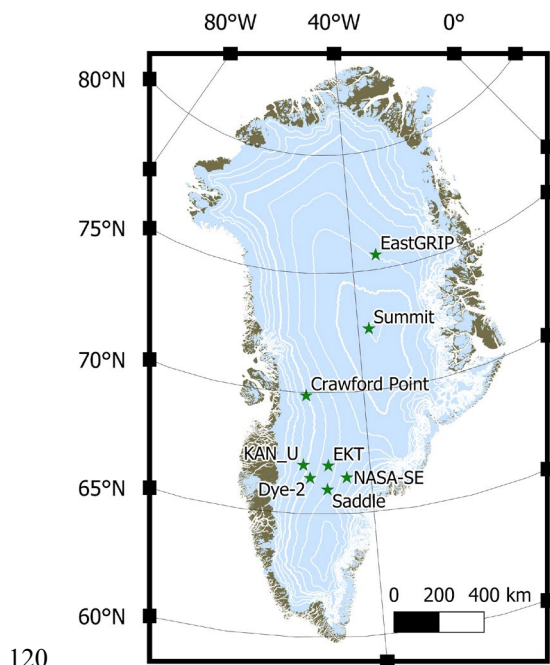


Figure 1: FirnCover station locations in Greenland. White lines are 1000 m (thick) and 250 m (thin) elevation contours.

Table 1: FirnCover station locations and metadata.

Station name	Latitude (°)	Longitude (°)	Elevation (m)
KAN_U	67.00	-47.02	1840
Dye-2	66.47	-46.28	2119
EKT	66.99	-44.39	2361
Saddle	66.00	-44.50	2456
NASA-SE	66.48	-42.50	2370
Crawford Point	69.88	-46.99	1942
Summit	72.58	-38.50	3208
EastGrip	75.63	-35.94	2666

3.1. The FirnCover strainmeters

125 The main components of each FirnCover station were borehole strainmeters, which made daily measurements of borehole
 lengths. These used the “coffee-can” method (Hulbe and Whillans, 1994; Hamilton et al., 1998) to continuously monitor firn
 compaction, similar to the method used by Arthern et al. (2010). Each instrument was composed of a line with a weight
 attached to one end and connected to a spring-loaded potentiometer on the other end. The weight was anchored at the bottom
 of a borehole, and the potentiometer was placed at the top of the borehole. As the borehole shortened due to firn compaction,
 130 the potentiometer reeled in string to maintain tension (Figure 2), and a data logger recorded the length of string that had been
 reeled in.



135 2.

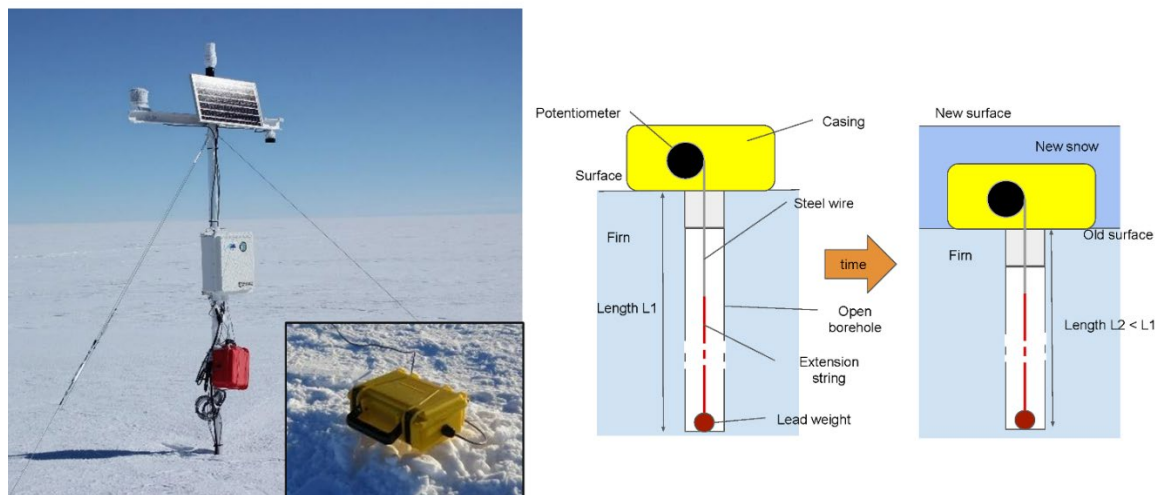


Figure 2: FirnCover station (left), strainmeter casing (inset), and strainmeter conceptual design (right)

140 The potentiometers were high-precision analog HX-PA units from Unimeasure, Inc. (Bend, Oregon) with a 2.032 m range. The end of the potentiometer's steel extension wire was attached to a Vectran string that extends to the bottom of the borehole. The string was anchored using a 0.226 kg lead weight. Each potentiometer was independently calibrated to accurately measure, within ± 1 mm, the length of the extension wire that was pulled out of the potentiometer. The potentiometer was enclosed in a weatherproof plastic case with an opening at the bottom. To stabilize the instrument atop the borehole, it was installed atop a
145 0.61 m² white PVC plastic platform. A section of PVC pipe (0.1-0.7 m long) was attached to the bottom of the casing and inserted in the top of the borehole to prevent the collapse of the top of the borehole and keep the instrument in place. The line lowered in the borehole was covered with hydrophobic lithium grease to prevent water from refreezing on it and to keep the line from snagging on the instrument or freezing to the side of the borehole.

150 To install each instrument, a borehole was drilled into the snow and firn using a Kovacs (diameter 9 cm) coring drill. The weighted Vectran string was then lowered into the borehole, and the potentiometer platform was placed atop of the borehole (Figure 2). The length of the string was set so that the potentiometer's steel cable was near its full extension, maximizing the distance over which the borehole shortening could be observed. Some instruments were installed on the surface and thus measured both the compaction of near-surface snow and underlying firn. Other instruments were installed at the bottom of
155 snow pits, beneath the annual layer of snow, to measure the compaction of the underlying firn only. In dry-snow regions



(Summit, EastGRIP) all instruments were installed directly on the surface, while instruments in the percolation zone were mixed between surface and snow-pit installations. The depth of each borehole was measured both along the core (by reassembling core segments on the surface) and by using the Vectran line to directly measure the borehole. Instruments #1-10, installed in 2013, use the approximate core length (as borehole length was not measured); the remaining instruments use the measured borehole length. Borehole and core-length measurements typically agreed to within 0-8 cm.

Table 2: FirnCover instrument metadata.

Site	Instrument ID	Recording start date	Recording end date	Initial Depth of borehole top (m)	Initial Depth of borehole bottom (m)
Crawford Point	22	27 May 2015	10 October 2018	1.03	17.33
	23	26 May 2015	10 October 2018	0	2.1
	24	27 May 2015	10 October 2018	1.09	9.38
	25	27 May 2015	10 October 2018	1.13	5.17
	42	17 May 2016	10 October 2018	0	18.09
	48	23 May 2017	10 October 2018	0	22.3
Dye-2	4	09 May 2013	4 September 2019	0	2
	5	09 May 2013	4 September 2019	1.35	11.35
	6	09 May 2013	4 September 2019	1.35	17.35
	21	21 May 2015	4 September 2019	0.85	18.85
	39	10 May 2016	4 September 2019	0	17.3
	47	11 May 2017	4 September 2019	0	22.85
EKT	7	19 May 2013	4 September 2019	0	2
	8	19 May 2013	4 September 2019	1.25	6.25
	9	19 May 2013	4 September 2019	1.25	11.25
	10	19 May 2013	4 September 2019	1.25	17.25
	12	8 May 2015	4 September 2019	0.9	14.9
	36	3 May 2016	31 July 2019	0	17.95



	44	5 May 2017	4 September 2019	0	22.24
EastGrip	26	28 May 2015	10 October 2018	0	15.83
	27	28 May 2015	10 October 2018	0	4.12
	28	29 May 2015	10 October 2018	0	8.05
	29	29 May 2015	10 October 2018	0	15.53
	40	16 May 2016	10 October 2018	0	16.28
	49	18 May 2017	10 October 2018	0	20.38
KAN_U	1	30 April 2013	9 May 2019	1.2	6.2
	2	30 April 2013	9 May 2019	0	2
	3	30 April 2013	9 May 2019	1.2	20.5
	11	05 May 2015	9 May 2019	0.64	14.14
	35	29 Apr 2016	9 May 2019	0	16.51
	43	28 Apr 2017	9 May 2019	0.78	22.86
NASA SE	13	12 May 2015	28 May 2018	0	16.4
	14	12 May 2015	28 May 2018	0	2.05
	15	12 May 2015	20 May 2018	0	8
	16	12 May 2015	28 May 2018	0	16.2
	45	6 May 2017	28 May 2018	0	22.17
Saddle	17	16 May 2015	31 Aug 2017	0	16.1
	18	16 May 2015	31 Aug 2017	0	2.03
	19	16 May 2015	31 Aug 2017	0	8.17
	20	16 May 2015	31 Aug 2017	0	16.3
	38	6 May 2016	31 Aug 2017	0	18.53
	46	8 May 2017	31 Aug 2017	0	22.34
Summit	30	29 May 2015	7 October 2018	0	15.73



	31	29 May 2015	7 October 2018	0	4.23
	32	29 May 2015	7 October 2018	0	7.77
	33	30 May 2015	7 October 2018	0	15.79
	41	17 May 2016	7 October 2018	0	16.08
	50	21 May 2017	7 October 2018	0	21.99

3.2. Air temperature, surface height and firn temperature observations

165 Each FirnCover station was equipped with a Campbell L109 air-temperature thermistor with 6-plate radiation shield, which
measured air temperature hourly at approximately 2 m ground height. Snow-surface height was measured from 2015 onward
with a SR50 sonic-ranging sensor mounted on the tower cross-beam. A string of 24 10-K Ω resistance-temperature diodes
(RTDs, from Omega sanitary, Class A, IEC 60751 standard) measured firn temperatures from 0 to approximately 14 m depth
(every 0.5 m from 0-10 m depth, every 1 m thereafter). The manufacturer-stated precision of the RTDs is $\pm 0.2^\circ\text{C}$. Some RTD-
170 string boreholes were less than 14 m due to challenges clearing chips from the boreholes. RTD measurements are corrected
for wire resistance (by measuring across a 25th bare wire without an RTD), and measured resistances are converted to
temperature using formulae provided by the RTD manufacturer. The initial installation depths of each RTD string are noted in
the FirnCover_Station_Metadata data table (Table A5). The daily depth of each thermistor is calculated by adding the original
installation depth to the snow depth measured by the sonic ranging sensor.

175

3.3. Firn core and snow pit observations

Firn cores were recovered from each of the FirnCover strainmeter boreholes. To understand the structure of the firn at each
FirnCover instrument, the cores were visually inspected for stratigraphic layers (ice lenses, etc.) at ~ 1 cm vertical resolution,
and cut into segments to measure density at ~ 10 cm resolution. At some sites where multiple FirnCover instruments were
180 installed in the same visit, only one core was logged and nearby boreholes were assumed to have similar stratigraphy and
density profiles. Density profiles from all cores logged by FirnCover field campaigns are included in the 2018 release of
NASA's SumUp dataset (Montgomery et al., 2018). The table "Compaction_Instrument_Metadata" (Table 3 and A7) give the
name of each FirnCover instrument's corresponding density profile in the SumUp dataset, as well as whether that
density/stratigraphy profile was observed in the same borehole as the instrument was installed or in an adjacent borehole within
185 10 m of the instrument.



4. Dataset structure and handling

The FirnCover dataset is organized in a single .hdf5 file, which comprises four data tables and three metadata tables. Table 3 gives a summary of the data tables, and tables A1 to A7 detail the variables contained in each table.

190 **Table 3: Overview of the FirnCover data tables**

Table name	Content	Further details in
Compaction_Daily	site name, daily timestamp, instrument ID, compaction ratio, potentiometer wire correction ratio, potentiometer cable length, compaction borehole length, top and bottom depth	Table A1
Air_Temp_Hourly	Site, hourly timestamp, air temperature	Table A2
Meteorological_Daily	site name, daily timestamp, battery minimum and maximum voltage, panel mean temperature, air hourly minimum, median and maximum temperature, sonic ranger quality raw and corrected distance, raw and interpolated snow depth	Table A3
Firn_Temp_Daily	site name, daily timestamp, thermistor average and maximum resistance value, uncorrected and corrected temperature value, average resistance of the cable used for correction, depth of the sensors	Table A4
Station_Metadata	site name, iridium URL, latitude, longitude, installation date, comments, thermistor string number, thermistor installation date, number of thermistors usable, depths at installation, direction and distance from tower	Table A5
Station_Visit_Notes	site name, date of visit, notes from each visit.	Table A6
Compaction_Instrument_Metadata.	instrument ID, site name, installation date, borehole top and bottom depth from surface, initial length, direction	Table A7



	and distance from tower, borehole ID in SUMup firn density dataset	
--	--	--

The first records of compaction for each strain meter may be subject to error due to settling effects. For the analyses presented here, we discard the first month of recordings for each instrument. This number is based on data from an instrument at KAN_U that was installed in a borehole comprising solid ice, which would be expected to have zero compaction but is still subject to instrument settling. That instrument registered a compaction signal for approximately one month before recording zero compaction for the remainder of its observations. We leave data from the initial month in the dataset so that more delicate filtering may allow the recovery of more observation within that period, but we recommend to potential users that it be discarded.

Some compaction data was read directly from the station’s data logger in 32-bit floating point format. For measurements where data tables were unable to be directly read due to lack of re-visit, data summaries from Iridium transmissions were used with 16-bit floating point values. Due to the limited data resolution, borehole lengths recorded from Iridium transmissions exhibit a 2 mm stepwise discretization rather than smooth continuous measurements. This can influence compaction rates when computed as derivatives of borehole lengths over time. In the present analysis, we use a two-month-wide running mean to smooth the borehole length. This filtering removes most of the noise, but it may also smooth part of seasonal changes of compaction rates. The dataset includes the unfiltered data to allow users to use their own filtering strategy.

Four of the stations had periods when the entire station was not recording data. These were: Summit, from 21-May-2017 to 23-August-2017; EKT, from 11-May-2017 to 18-May-2018; KAN_U from 07-November-2017 to 30-April-2018 and from 13-January-2019 to 20-February-2019; and Saddle from 30-May-2015 to 05-May-2016. For a number of the instruments, there are periods of data that we consider suspicious. These are listed in Table 4. We exclude these suspicious data from our analysis in Section 5. They are included in the released dataset, but we advise using caution when using them.

Table 4. Periods with suspicious recordings removed from the analysis.

Instrument ID	Failure start date	Failure end date
13	20 February 2018	-
10	29 July 2019	-
42	-	14 November 2017
48	-	18 November 2017

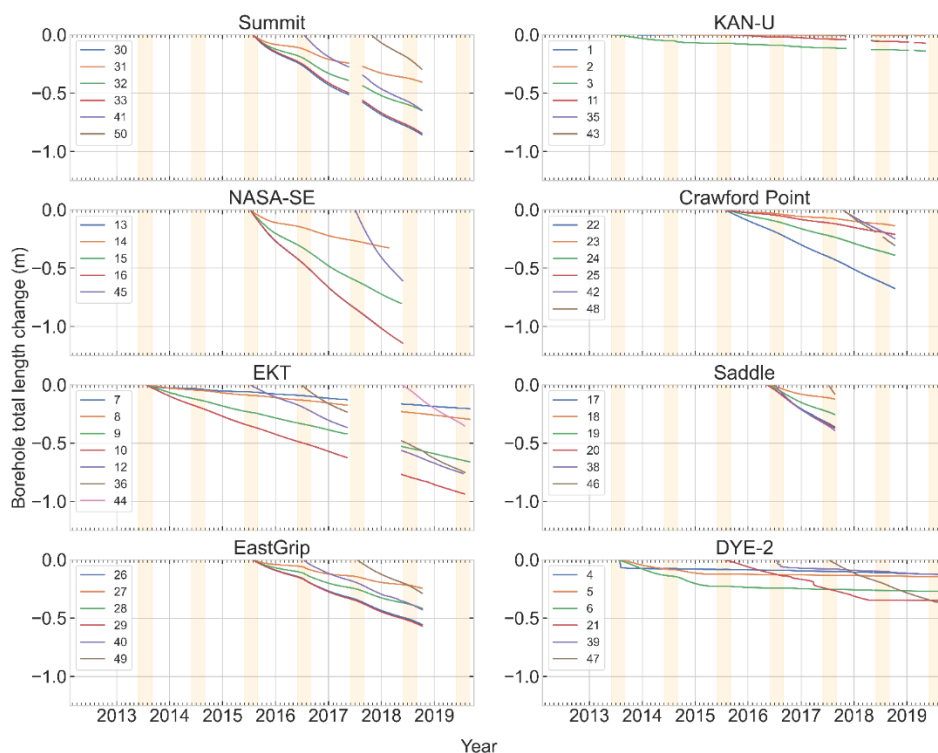


48	27 May 2018	19 July 2018
1	-	1 December 2013
35	-	1 September 2016
43	16 July 2018	-

215

5. Data overview and preliminary analysis

Figure 3 shows the change in borehole length measured by each potentiometer at the eight sites. At all sites, a fast initial shortening is followed by a steadier borehole shortening period. NASA-SE shows the steepest borehole shortening with instruments #36 installed in 2017 and also the largest change in borehole length, -1.25m for the 16.2 m long borehole #16 installed in 2015. This rapid shortening of the borehole largely stems from the climatic conditions at NASA-SE because: (1) high accumulation rates create a thick, low-density layer near the surface (which has a lower effective viscosity), and (2) the fast build-up of new snow atop the borehole increases overburden pressure quickly, which speeds the densification rate. At Dye-2 and KAN-U, the borehole shortening is the least pronounced. This is due to higher air temperatures, higher melt and lower snowfall at these sites; together they lead to higher firn density and ice content which decreases compaction rate. At other sites, total borehole shortening ranges from a few centimeters to about a meter at EKT depending on the climatic conditions and the length of the observation period. Most sites, but especially Summit and EastGrip, show a seasonality in the borehole shortening rate: boreholes shorten faster (steeper curve in Figure 4) during and after summer months (orange shaded areas) and slower (flattening of curves in Figure 4) in the winter/spring months.



230

Figure 3. Borehole total length changes relative to installation depth plus 120 days. June-July-August are highlighted in orange. Note that the boreholes at each site had different initial lengths, so compaction is not expected to be the same for all holes at a particular site.

235 The difference between sites can be further investigated by looking at the compaction rates, which are calculated by taking the time derivative of the borehole length data (Figure 4). As discussed above, NASA-SE shows the largest daily changes and KAN-U the lowest. At each site, instruments installed in deeper boreholes show larger magnitude of daily compaction compared to shorter instruments. The faster compaction after the installation of the instrument appears as peaks in firm compaction rates in Figure 4. Since we already discard the settling period of the instrument, we attribute these faster initial
240 compaction rates to the high potential for deformation of low-density, relatively new snow/firm in which the instruments are installed. Faster compaction during the first summer following the installation of the instruments also stems from the conduction of warmer surface temperatures down to the instrument during summer. These warmer firm temperatures during summer increase the firm compaction rates. In spite of the smoothing applied, KAN-U, Crawford Point, EKT and Dye-2 still show notable noise. They are the sites that undergo the highest melt; we hypothesize that this noise is due to interaction between
245 meltwater and the borehole. Targeted noise removal strategies may be necessary at these sites for any potential users. As mentioned previously, daily compaction rates at KAN-U are lower than at other sites due to the presence of a ~5 m thick ice



250

slab at that site. The seasonality of the daily compaction rates is clearly visible at the dry snow sites, Summit and EastGRIP, but also at sites in the percolation areas: NASA-SE, Crawford Point, EKT and Saddle. Daily compaction rates peak in the autumn and reach a minimum at the end of the winter. The delay between the highest (resp. lowest) surface temperatures in summer (resp. winter) and the highest (resp. lowest) compaction rates is due to the time the surface temperatures need to diffuse down to the depth of the firn that the instrument is measuring.

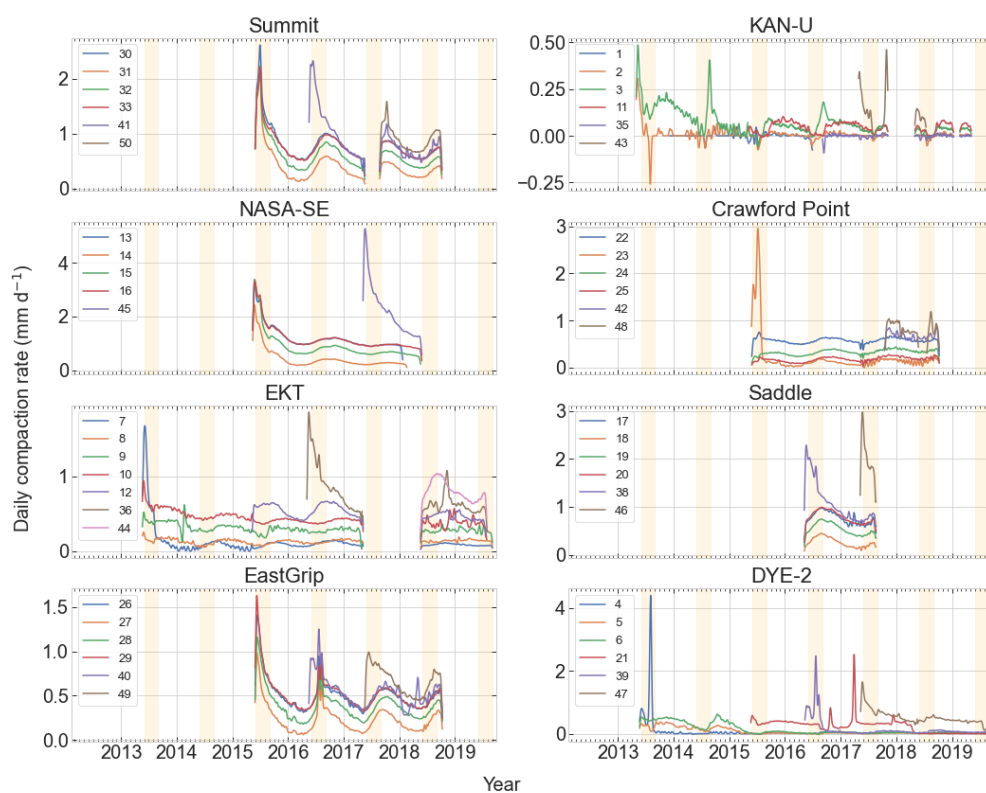
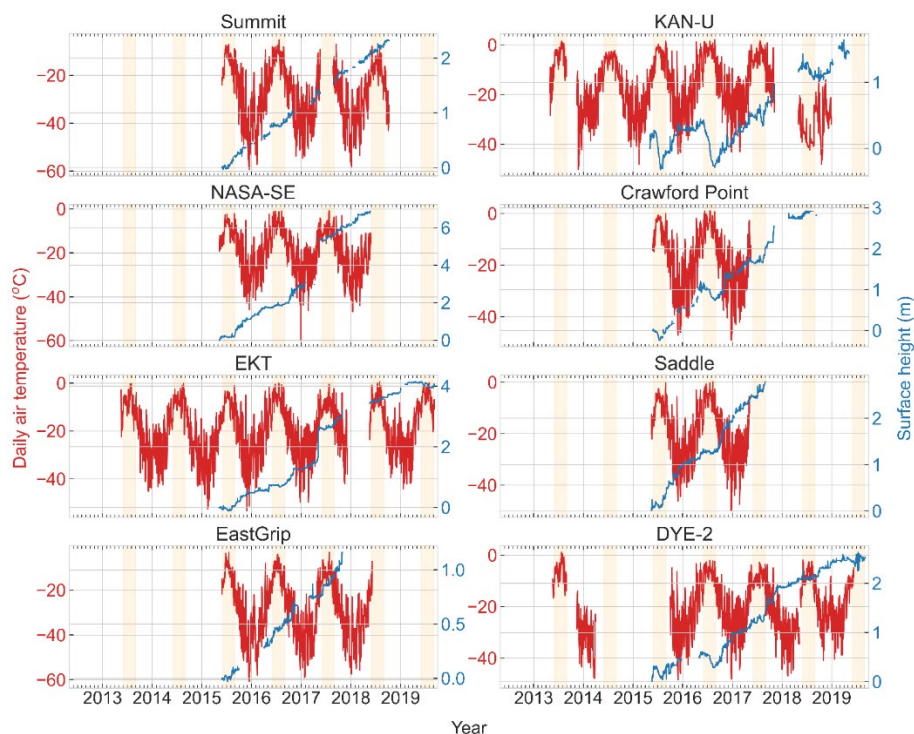


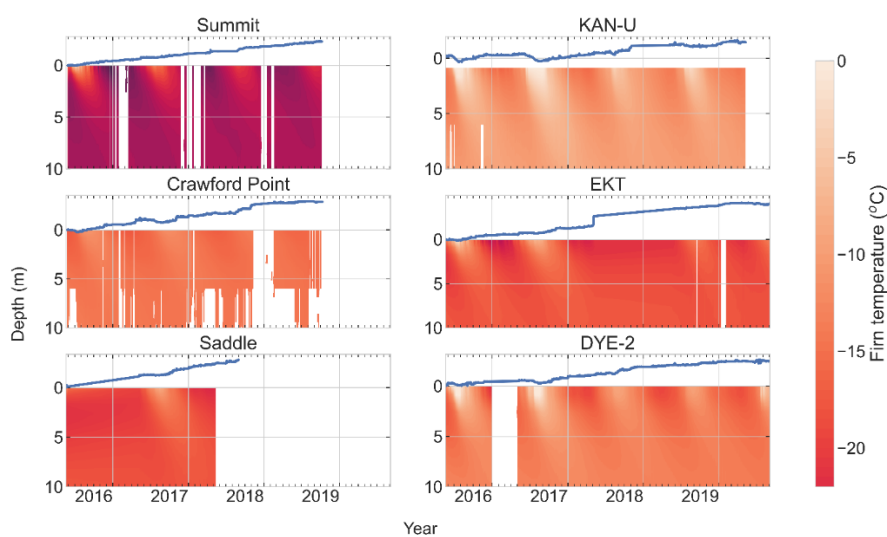
Figure 4. Smoothed daily compaction rates. June-July-August are highlighted in orange. Note the different y-axes. The different curves represent different depth intervals as reported in Table 2.

255

The FirnCover dataset also includes air temperature, surface height, and firn-temperature measurements (at all sites except EastGRIP and NASA-SE); these data enable us to relate the compaction rates to each year's weather conditions (Figures 5 and 6).



260 **Figure 5.** Daily air temperature (red line, left axis) and surface height (blue line, right axis). June-July-August are highlighted in orange. Note the different y-axes.



265 **Figure 6.** Firn temperatures and surface height (blue solid line) observed at the FirnCover stations.



The firn temperature measurements, in particular, allow analyses using the actual firn conditions rather than using average air temperature as a proxy for firn temperature, which is commonly done. The comparison of average air temperature and interpolated 10m firn temperatures indicate that they are rarely equivalent (Table 4). At Summit, the 10m firn temperatures are 2.6 °C lower than the average air temperature. This is due to strong near-surface atmospheric inversion and radiative cooling of the surface (e.g. Miller et al., 2017). At all the other sites, the 2 m firn temperature is higher than the average air temperature. We attribute this to meltwater percolation and latent heat release at depth (e.g. Humphrey et al., 2012). This difference is largest at KAN-U where the firn is 7°C warmer than the average air temperature. At Saddle, the firn temperature is within a degree of the average air temperature. We interpret this as the neutralization of the two processes mentioned above: heat loss through radiative cooling at the surface and latent heat release during meltwater refreezing. This site-specific difference between 10 m firn temperature and average air temperature shows the limitation of firn compaction parameterizations that use air temperature as a proxy for firn temperature and how these parameterizations perform outside of their training site.

Table 4. Average air temperature, 10 m firn average temperatures and difference between the two.

Site	Average 10 m firn temperature (°C)	Average air temperature (°C)	Difference (°C)
Summit	-28.8	-26.20	-2.64
KAN_U	-9.5	-16.60	7.06
Crawford Point	-14.4	-16.20	1.78
EKT	-17.9	-20.20	2.30
Saddle	-17.9	-18.10	0.17
DYE-2	-13.2	-19.20	5.97

6. Summary remarks

We present data from 50 strainmeters installed at eight sites located in different climatic zones of the Greenland ice sheet and covering the 2013-2019 period. Additional surface and firn measurements available at each of the FirnCover sites are firn density, air temperature, surface height and firn temperatures. These data will allow future work to investigate the interannual and seasonal response of firn compaction to surface and subsurface conditions. We also note that several other measurements are available at some of the FirnCover sites: at KAN-U the PROMICE automatic weather station has been operating since 2009 (Ahlstrøm et al., 2008); at Crawford Point, Saddle, NASA-SE, Summit and Dye-2, GC-Net weather stations document the history of these sites back to the 1990s and are still operating. At Summit, extensive instrumentation is measuring the atmospheric conditions and the surface energy budget (e.g. Miller et al., 2017). At Dye-2, upward looking Ground Penetrating Radar (Heilig et al., 2018) and time-domain resistivity probes (Samimi et al., 2020) are also available for the 2016 melt season to detail meltwater percolation. These measurements, combined with the FirnCover compaction data, potentially allow



investigations of how meltwater affects firn compaction. The FirnCover dataset will help to evaluate and calibrate firn models and help reduce uncertainty when using these models to interpret satellite altimetry measurements or calculating the past, current and future mass balance of polar ice sheets. The dataset can be found here: <https://www.doi.org/10.18739/A25X25D7M>.

295

7. Data Availability

The FirnCover dataset is available at <https://www.doi.org/10.18739/A25X25D7M> (MacFerrin et al., 2021). The firn density profiles at the firn cover sites are available here: <https://doi.org/10.18739/A26D5PB2S> (Koenig and Montgomery, 2019).

8. Code Availability

300 All the scripts used to load, process and plot the FirnCover dataset are available here: <https://github.com/BaptisteVandecrux/FirnCover>.

9. Acknowledgements

305 The majority of this work, including instrumentation and station visits, was funded by NASA awards NNX15AC62G and NNX10AR76G. All authors acknowledge the work and efforts of multiple field logistic partners and team members for their essential help in maintaining the datasets and instruments: K. Alley, C. Charalampidis, W. Colgan, F. Covi, A. Crawford, M. Eijkelboom, S. Grigsby, A. Heilig, D. Hill, H. Machguth, S. Marshall, A. Rennermalm, S. Samimi, T. Snow, A. Sommers, D. van As, the Summit Station scientific team, the EastGrip team and Polar Field Services.

10. Author contribution

310 MM conducted the conceptualization, funding acquisition, the methodology, the field investigation and the data curation. CMS participated to the conceptualization, funding acquisition, field investigation, formal analysis and visualization. BV participated to the field investigation, formal analysis and visualization. EW and WA participated to the funding acquisition and supervision. All authors contributed to the manuscript preparation.

11. Competing interests

315 The authors declare that they have no conflict of interest.



12. Appendix

Table A1: Compaction_Daily table. Stores daily compaction records for each FirnCover instrument.

Field Name	Comments
sitename	Name of the FirnCover site
daynumber YYYYMMDD	Year, month, date of the measurement
Compaction_Instrument_ID	linked to “Compaction_Instrument_Metadata” table
Compaction_Ratio_Med	The ratio of the compaction line measurement (fraction of total instrument cable length), values 0 to 1, inclusive. Uses a median value of six daily measurements.
Compaction_Wire_Correction_Ratio_Med	The ratio of the wire resistance as a fraction of the total line resistance. Values 0 to 1, inclusive (typically below 0.001).
Compaction_Cable_Distance_m	Distance the instrument wire is extended, typically 0-2 m (up to 5 m for extended-cable instruments)
Compaction_Borehole_Length_m	Length of the borehole at that time step. Combines the updated cable length with the initial borehole length.
Borehole_Depth_Top_m	Depth from the surface to the top of the borehole at that time step, combining the initial borehole depth (0 for the surface) and the Sonic Ranger snow depth measurement.
Borehole_Depth_Bottom_m	Depth from the surface to the bottom of the borehole. Computed as “Borehole_Depth_Top_m” + “Compaction_Borehole_Length_m”

320 **Table A2: Air_Temp_Hourly table**

Field Name	Comments
sitename	Name of the FirnCover site
daynumber YYYYMMDD	Year, month, date of the measurement
hournumber HH	Hour of the day (0 through 23)
AirTemp_C	~2 m air temperature at that hour, measured by the shielded L109 thermistor, in °C. Actual height of the temperature measurement can be derived by adding 28 cm to the Sonic Ranger height in “FirnCover Meteorological Daily DataTable”

Table A3: Meteorological_Daily table

Field Name	Comments
------------	----------



sitename	Name of the FirnCover site
daynumber YYYYMMDD	Year, month, date of the measurement
BattV_min_V	Minimum station battery voltage for the day
BattV_max_V	Maximum station battery voltage for the day
PanelTemp_mean_C	Mean daily temperature (°C) measured on the data logger inside the logger box
AirTemp_min_C	Minimum daily air temperature (°C) measured hourly
AirTemp_max_C	Maximum daily air temperature (°C) measured hourly
SonicRangeQuality	The quality score value of the Sonic Ranging sensor, chosen as the highest-quality of 24 daily measurements. Ranges from 162 to 600 with good quality scores below 210.
SonicRangeQualityCode	0=Good, 1=Questionable, 2=Poor, 3=No Measurement
SonicRangeDist_Raw_m	The raw distance measured by the sonic ranger, before temperature correction.
SonicRangeAirTemp_C	The air temperature at the time of the sonic ranger measurement.
SonicRangeDist_Corrected_m	The corrected distance measured by the sonic ranger.
Accum_Snow_Depth_m	The accumulated snow depth since the instruments' installation, corrected for tower raises upon revisits.

325

Table A4: Firn_Temp_Daily table

Field Name	Comments
sitename	Name of the FirnCover site
daynumber YYYYMMDD	The day of the reading
RTD Ohms Avg	Average RTD resistance reading
RTD Ohms Max	Maximum RTD resistance reading
RTD Temp Avg Uncorrected C	Average RTD temperature reading (deg C)
RTD Temp Max Uncorrected C	Maximum RTD temperature reading (deg C)
RTD Line Correction Ohms Avg	The line correction
RTD_Temp_Avg_Corrected_C	Average RTD temperature reading (deg C), w/ adjustment for wire resistance
RTD_Temp_Max_Corrected_C	Maximum RTD temperature reading (deg C), w/ adjustment for wire resistance

330 **Table A5: Station_Metadata table**

Field Name	Comments
sitename	Name of the FirnCover site
iridium_URL	The online URL where transmissions are collected



latitude	The WGS84 latitude of the station upon installation
longitude	The WGS84 longitude of the station upon installation
installation_daynumber_YYYYMMDD	The day the station was installed.
comments	General comments about the station upon its installation.
RTD_stringnumber	The string serial number of the RTD string installed at the station.
RTD_installation_daynumber_YYYYMMDD	The day at the RTD was installed at the station.
RTD_top_usable_RTD_num	Number (from the top) of the first usable RTD sensor. Non-usable sensors could not be inserted in the snow and were left lying on the surface.
RTD_depths_at_installation_m	The 24-length depths of each RTD at installation.
RTD_direction_from_tower_degrees	The compass direction (non-corrected for declination) of the station tower to the RTD string.
RTD_distance_from_tower_m	The distance from the station tower to the RTD string.

Table A6: Station_Visit_Notes table.

Field Name	Comments
sitename	Name of the FirnCover site
daynumber_YYYYMMDD	Day of the visit
visit_notes	Notes about the site visit or revisit.

335

Table A7: Compaction_Instrument_Metadata table. Installation depths and positions of each FirnCover compaction instrument.

Field Name	Comments
instrument_ID	Unique identification number of the instrument
sitename	Name of the FirnCover site
installation_daynumber_YYYYMMDD	Date that the instrument was installed.
borehole_top_from_surface_m	The top of the borehole from the surface upon installation, in m. (0 for surface, negative numbers for beneath the surface)
borehole_bottom_from_surface_m	The depth from the surface to the bottom of the borehole, in m
borehole_initial_length_m	The length of the borehole, in m
instrument_has_wire_correction	Whether the instrument installed has a wire-resistance correction sensor installed, or not.
direction_from_tower_degrees	The compass direction (not corrected for declination) from the tower to the instrument.
distance_from_tower_m	The distance (in m) from the tower to the instrument.
borehole_ID	The identifying name of the core taken from the borehole, where stratigraphy and density were measured (names consistent with cores in the NASA SumUp dataset).



borehole_ID_is_direct	A "direct" (True) core density profile came straight from that borehole. If "indirect" (False), that core was not profiled for density directly, and this links to a nearby. Adjacent core measured at the same time, typically within 10-20 meters distance.
-----------------------	---

13. References

- Adolph, A. C. and Albert, M. R.: Gas diffusivity and permeability through the firn column at Summit, Greenland: Measurements and comparison to microstructural properties, *Cryosphere*, 8(1), 319–328, <https://www.doi.org/10.5194/tc-8-319-2014>, 2014.
- Arthern, R. J., Vaughan, D. G., Rankin, A. M., Mulvaney, R. and Thomas, E. R.: In situ measurements of Antarctic snow compaction compared with predictions of models, *J. Geophys. Res. Earth Surf.*, 115(3), <https://www.doi.org/10.1029/2009JF001306>, 2010.
- 345 Bader, H.: Sorge's Law of Densification of Snow on High Polar Glaciers, *J. Glaciol.*, 2(15), 319–323, <https://www.doi.org/10.3189/s0022143000025144>, 1954.
- Benson, C. S.: Stratigraphic studies in the snow and firn of the Greenland Ice Sheet, U.S. Snow, Ice and Permafrost Research Establishment, Research Report 70, 1962.
- Box, J. E., Bromwich, D. H., Veenhuis, B. A., Bai, L. S., Stroeve, J. C., Rogers, J. C., Steffen, K., Haran, T. and Wang, S. H.: Greenland ice sheet surface mass balance variability (1988-2004) from calibrated polar MM5 output, *J. Clim.*, 19(12), 2783–2800, <https://www.doi.org/10.1175/JCLI3738.1>, 2006.
- Brown, J., Bradford, J., Harper, J., Pfeffer, W. T., Humphrey, N. and Mosley-Thompson, E.: Georadar-derived estimates of firn density in the percolation zone, western Greenland ice sheet, *J. Geophys. Res. Earth Surf.*, 117(1), 1–14, <https://www.doi.org/10.1029/2011JF002089>, 2012.
- 355 Brun, E.: Investigation on Wet-Snow Metamorphism in Respect of Liquid-Water Content, *Ann. Glaciol.*, 13, 22–26, <https://www.doi.org/https://www.doi.org/10.3189/S0260305500007576>, 1989.
- Van Den Broeke, M. R., Enderlin, E. M., Howat, I. M., Kuipers Munneke, P., Noël, B. P. Y., Jan Van De Berg, W., Van Meijgaard, E. and Wouters, B.: On the recent contribution of the Greenland ice sheet to sea level change, *Cryosphere*, 10(5), 1933–1946, <https://www.doi.org/10.5194/tc-10-1933-2016>, 2016.
- 360 Csatho, B. M., Schenk, A. F., van der Veen, C. J., Babonis, G., Duncan, K., Rezvanbehbahani, S., van den Broeke, M. R., Simonsen, S. B., Nagarajan, S. and van Angelen, J. H.: Laser altimetry reveals complex pattern of Greenland Ice Sheet dynamics, *Proc. Natl. Acad. Sci.*, 111(52), 18478–18483, <https://www.doi.org/10.1073/pnas.1411680112>, 2014.
- Forster, R. R., Box, J. E., Van Den Broeke, M. R., Miège, C., Burgess, E. W., Van Angelen, J. H., Lenaerts, J. T. M., Koenig, L. S., Paden, J., Lewis, C., Gogineni, S. P., Leuschen, C. and McConnell, J. R.: Extensive liquid meltwater storage in firn within the Greenland ice sheet, *Nat. Geosci.*, 7(2), 95–98, <https://www.doi.org/10.1038/ngeo2043>, 2014.



- Goujon, C., Barnola, J. M. and Ritz, C.: Modelling the densification of polar firn including heat diffusion: Application to close-off characteristics and gas isotopic fractionation for Antarctica and Greenland sites, *J. Geophys. Res. D Atmos.*, 108(24), <https://www.doi.org/10.1029/2002JD003319>, 2003.
- 370 Hamilton, G. S., Whillans, I. M. and Morgan, P. J.: First point measurements of ice-sheet thickness change in Antarctica, *Ann. Glaciol.*, 27, 125–129, <https://www.doi.org/10.3189/1998AoG27-1-125-129>, 1998.
- Hamilton, G. S. and Whillans, I. M.: Local rates of ice-sheet thickness change in Greenland, *Ann. Glaciol.*, 35, 79–83, <https://www.doi.org/10.3189/172756402781817383>, 2002.
- 375 Herron, M. M. and Langway, C. C.: Firn densification: an empirical model., *J. Glaciol.*, 25(93), 373–385, <https://www.doi.org/10.1017/S0022143000015239>, 1980.
- IPCC: Climate Change 2013: Climate Change 2013: The Physical Science Basis. Contribution of Working Group I to the Fifth Assessment Report of the Intergovernmental Panel on Climate Change, edited by T. F. Stocker, D. Qin, G. K. Plattner, M. M. B. Tignor, S. K. Allen, J. Boschung, A. Nauels, Y. Xia, V. Bex, and P. M. Midgley, Cambridge University Press, Cambridge, United Kingdom and New York, NY, USA., 2013.
- 380 Koenig, L. and Montgomery, L.: Surface Mass Balance and Snow Depth on Sea Ice Working Group (SUMup) snow density subdataset, Greenland and Antarctica, 1950-2018, Arctic Data Center, <https://www.doi.org/10.18739/A26D5PB2S>, 2019.
- Li, J. and Zwally, H. J.: Response times of ice-sheet surface heights to changes in the rate of Antarctic firn compaction caused by accumulation and temperature variations, *J. Glaciol.*, 61(230), 1037–1047, <https://www.doi.org/10.3189/2015JoG14J182>, 2015.
- 385 MacFerrin, M., Machguth, H., As, D. van, Charalampidis, C., Stevens, C. M., Heilig, A., Vandecrux, B., Langen, P. L., Mottram, R., Fettweis, X., Broeke, M. R. van den, Pfeffer, W. T., Moussavi, M. S. and Abdalati, W.: Rapid expansion of Greenland’s low-permeability ice slabs, *Nature*, 573(7774), 403–407, <https://www.doi.org/10.1038/s41586-019-1550-3>, 2019.
- MacFerrin, M., Stevens, C. M., Vandecrux, B.: The Greenland Firn Compaction Verification and Reconnaissance (FirnCover) Dataset, 2013-2019. Arctic Data Center, <https://www.doi.org/10.18739/A25X25D7M>, 2021.
- 390 Machguth, H., Macferrin, M., Van As, D., Box, J. E., Charalampidis, C., Colgan, W., Fausto, R. S., Meijer, H. A. J., Mosley-Thompson, E. and Van De Wal, R. S. W.: Greenland meltwater storage in firn limited by near-surface ice formation, *Nat. Clim. Chang.*, 6(4), 390–393, <https://www.doi.org/10.1038/nclimate2899>, 2016.
- McGrath, D., Colgan, W., Bayou, N., Muto, A. and Steffen, K.: Recent warming at Summit, Greenland: Global context and implications, *Geophys. Res. Lett.*, 40(10), 2091–2096, <https://www.doi.org/10.1002/grl.50456>, 2013.
- 395 McMillan, M., Leeson, A., Shepherd, A., Briggs, K., Armitage, T. W. K., Hogg, A., Kuipers Munneke, P., van den Broeke, M., Noël, B., van de Berg, W. J., Ligtenberg, S., Horwath, M., Groh, A., Muir, A. and Gilbert, L.: A high-resolution record of Greenland mass balance, *Geophys. Res. Lett.*, 43(13), 7002–7010, <https://www.doi.org/10.1002/2016GL069666>, 2016.
- Miller, N. B., Shupe, M. D., Cox, C. J., Noone, D., Persson, P. O. G. and Steffen, K.: Surface energy budget responses to radiative forcing at Summit, Greenland, *Cryosphere*, 11(1), 497–516, <https://www.doi.org/10.5194/tc-11-497-2017>, 2017.
- 400 Montgomery, L., Koenig, L. and Alexander, P.: The SUMup Dataset: Compiled measurements of surface mass balance components over ice sheets and sea ice with preliminary analysis over Greenland, *Earth Syst. Sci. Data Discuss.*, (March), 1–31, <https://www.doi.org/10.5194/essd-2018-21>, 2018.



- Morris, E. M. and Wingham, D. J.: Densification of polar snow: Measurements, modeling, and implications for altimetry, *J. Geophys. Res. Earth Surf.*, 119(2), 349–365, <https://www.doi.org/10.1002/2013JF002898>, 2014.
- 405 Mottram, R., Simonsen, S. B., Svendsen, S. H., Barletta, V. R., Sørensen, L. S., Nagler, T., Wuite, J., Groh, A., Horwath, M., Rosier, J., Solgaard, A., Hvidberg, C. S. and Forsberg, R.: An Integrated View of Greenland Ice Sheet Mass Changes Based on Models and Satellite Observations, *Remote Sens.*, 11(12), 1–26, <https://www.doi.org/10.3390/rs11121407>, 2019.
- Munneke, P. K., Ligtenberg, S. R. M., Van Den Broeke, M. R., Van Angelen, J. H. and Forster, R. R.: Explaining the presence of perennial liquid water bodies in the firn of the Greenland Ice Sheet, *Geophys. Res. Lett.*, 41(2), 476–483, 410 <https://www.doi.org/10.1002/2013GL058389>, 2014.
- Nghiem, S. V., Hall, D. K., Mote, T. L., Tedesco, M., Albert, M. R., Keegan, K., Shuman, C. A., DiGirolamo, N. E. and Neumann, G.: The extreme melt across the Greenland ice sheet in 2012, *Geophys. Res. Lett.*, 39(20), 6–11, <https://www.doi.org/10.1029/2012GL053611>, 2012.
- Rasmussen, S. O., Abbott, P. M., Blunier, T., Bourne, A. J., Brook, E., Buchardt, S. L., Buizert, C., Chappellaz, J., Clausen, 415 H. B., Cook, E., Dahl-Jensen, D., Davies, S. M., Guillevic, M., Kipfstuhl, S., Laepple, T., Seierstad, I. K., Severinghaus, J. P., Steffensen, J. P., Stowasser, C., Svensson, A., Vallengonga, P., Vinther, B. M., Wilhelms, F. and Winstrup, M.: A first chronology for the north greenland eemian ice drilling (NEEM) ice core, *Clim. Past*, 9(6), 2713–2730, <https://www.doi.org/10.5194/cp-9-2713-2013>, 2013.
- Reeh, N.: A nonsteady-state firn-densification model for the percolation zone of a glacier, *J. Geophys. Res. Earth Surf.*, 113(3), 420 F03023, <https://www.doi.org/10.1029/2007JF000746>, 2008.
- Schwander, J., Sowers, T., Barnola, J. M., Blunier, T., Fuchs, A. and Malaizé, B.: Age scale of the air in the summit ice: Implication for glacial-interglacial temperature change, *J. Geophys. Res. Atmos.*, 102(16), 19483–19493, <https://www.doi.org/10.1029/97jd01309>, 1997.
- Schwander, J. and Stauffer, B.: Age difference between polar ice and the air trapped in its bubbles, *Nature*, 311(5981), 45–47, 425 <https://www.doi.org/10.1038/311045a0>, 1984.
- Shepherd, A., Ivins, E. R., Geruo, A., Barletta, V. R., Bentley, M. J., Bettadpur, S., Briggs, K. H., Bromwich, D. H., Forsberg, R., Galin, N., Horwath, M., Jacobs, S., Joughin, I., King, M. A., Lenaerts, J. T. M., Li, J., Ligtenberg, S. R. M., Luckman, A., Luthcke, S. B., McMillan, M., Meister, R., Milne, G., Mouginot, J., Muir, A., Nicolas, J. P., Paden, J., Payne, A. J., Pritchard, H., Rignot, E., Rott, H., Sørensen, L. S., Scambos, T. A., Scheuchl, B., Schrama, E. J. O., Smith, B., Sundal, A. V., Van 430 Angelen, J. H., Van De Berg, W. J., Van Den Broeke, M. R., Vaughan, D. G., Velicogna, I., Wahr, J., Whitehouse, P. L., Wingham, D. J., Yi, D., Young, D. and Zwally, H. J.: A reconciled estimate of ice-sheet mass balance, *Science* (80-.), 338(6111), 1183–1189, <https://www.doi.org/10.1126/science.1228102>, 2012.
- Smith, B., Fricker, H. A., Gardner, A. S., Medley, B., Nilsson, J., Paolo Nicholas Holschuh, F. S., Adusumilli, S., Brunt, K., Csatho, B., Harbeck, K., Markus, T., Neumann, T., Siegfried, M. R. and Jay Zwally, H.: Pervasive ice sheet mass loss reflects competing ocean and atmosphere processes, *Science* (80-.), 368(6496), 1239–1242, 435 <https://www.doi.org/10.1126/science.aaz5845>, 2020.
- Sørensen, L. S., Simonsen, S. B., Nielsen, K., Lucas-Picher, P., Spada, G., Adalgeirsdottir, G., Forsberg, R. and Hvidberg, C. S.: Mass balance of the Greenland ice sheet (2003–2008) from ICESat data - The impact of interpolation, sampling and firn 440 density, *Cryosphere*, 5(1), 173–186, <https://www.doi.org/10.5194/tc-5-173-2011>, 2011.
- Steffen, K. and Box, J.: Surface climatology of the Greenland ice sheet: Greenland Climate Network 1995–1999, *J. Geophys. Res. Atmos.*, 106(D24), 33951–33964, <https://www.doi.org/10.1029/2001JD900161>, 2001.



- 445 Tedesco, M., Fettweis, X., Mote, T., Wahr, J., Alexander, P., Box, J. E. and Wouters, B.: Evidence and analysis of 2012 Greenland records from spaceborne observations, a regional climate model and reanalysis data, *Cryosph.*, 7(2), 615–630, <https://www.doi.org/10.5194/tc-7-615-2013>, 2013.
- Van As, D., Fausto, R. S., Cappelen, J., Van De Wal, R. S. W., Braithwaite, R. J., Machguth, H., Charalampidis, C., Box, J. E., Solgaard, A. M., Ahlstrom, A. P., Haubner, K., Citterio, M. and Andersen, S. B.: Placing Greenland ice sheet ablation measurements in a multi-decadal context, *Geol. Surv. Denmark Greenl. Bull.*, 35, 71–74, <https://www.doi.org/10.34194/geusb.v35.4942>, 2016.
- 450 Vandecrux, B., Fausto, R. S., Langen, P. L., van As, D., MacFerrin, M., Colgan, W. T., Ingeman-Nielsen, T., Steffen, K., Jensen, N. S., Møller, M. T. and Box, J. E.: Drivers of Firn Density on the Greenland Ice Sheet Revealed by Weather Station Observations and Modeling, *J. Geophys. Res. Earth Surf.*, 123(10), 2563–2576, <https://www.doi.org/10.1029/2017JF004597>, 2018.
- 455 Vandecrux, B., MacFerrin, M., MacHguth, H., Colgan, W. T., Van As, D., Heilig, A., Max Stevens, C., Charalampidis, C., Fausto, R. S., Morris, E. M., Mosley-Thompson, E., Koenig, L., Montgomery, L. N., Miège, C., Simonsen, S. B., Ingeman-Nielsen, T. and Box, J. E.: Firn data compilation reveals widespread decrease of firn air content in western Greenland, *Cryosphere*, 13(3), 845–859, <https://www.doi.org/10.5194/tc-13-845-2019>, 2019.
- 460 Vandecrux, B., Fausto, R. S., Van As, D., Colgan, W., Langen, P. L., Haubner, K., Ingeman-Nielsen, T., Heilig, A., Stevens, C. M., MacFerrin, M., Niwano, M., Steffen, K. and Box, J. E.: Firn cold content evolution at nine sites on the Greenland ice sheet between 1998 and 2017, *J. Glaciol.*, 66(258), 591–602, <https://www.doi.org/10.1017/jog.2020.30>, 2020.
- Velicogna, I., Sutterley, T. C. and Van Den Broeke, M. R.: Regional acceleration in ice mass loss from Greenland and Antarctica using GRACE time-variable gravity data, *Geophys. Res. Lett.*, 41(22), 8130–8137, <https://www.doi.org/10.1002/2014GL061052>, 2014.
- 465 Zwally, H. J., Li, J., Brenner, A. C., Beckley, M., Cornejo, H. G., Marzio, J. Di, Giovinetto, M. B., Neumann, T. A., Robbins, J., Saba, J. L., Yi, D. and Wang, W.: Greenland ice sheet mass balance: Distribution of increased mass loss with climate warming; 2003–07 versus 1992–2002, *J. Glaciol.*, 57(201), 88–102, <https://www.doi.org/10.3189/002214311795306682>, 2011.